Journal of Zhejiang University-SCIENCE A (Applied Physics & Engineering)
ISSN 1673-565X (Print); ISSN 1862-1775 (Online)
www.jzus.zju.edu.cn; www.springerlink.com
E-mail: jzus@zju.edu.cn

A novel forced motion apparatus with potential applications in structural engineering*

Lin ZHAO[1,2], Xi XIE[1], Yan-yan ZHAN[1], Wei CUI[†‡2], Yao-jun GE[1,2],
Zheng-chun XIA[3], Sheng-qiao XU[4], Min ZENG[3]

[1]*State Key Laboratory of Disaster Reduction in Civil Engineering, Tongji University, Shanghai 200092, China*
[2]*Key Laboratory of Transport Industry of Wind Resistant Technology for Bridge Structures, Tongji University, Shanghai 200092, China*
[3]*China Railway Siyuan Survey and Design Group Co. Ltd., Wuhan 430063, China*
[4]*China Railway Engineering Design and Consulting Group, Beijing 100055, China*
[†]E-mail: cuiwei@tongji.edu.cn

Received Aug. 20, 2019; Revision accepted Dec. 3, 2019; Crosschecked June 12, 2020

Abstract: This paper reviews the development of forced motion apparatuses (FMAs) and their applications in wind engineering. A kind of FMA has been developed to investigate nonlinear and nonstationary aerodynamic forces considering the coupled effects of multiple degrees of freedom (DOFs). This apparatus can make section models to vibrate in a prescribed displacement defined by a numerical signal in time domain, including stationary and nonstationary movements with time-variant amplitudes and frequencies and even stochastic displacements. A series of validation tests show that the apparatus can re-illustrate various motions with enough precision in 3D coupled states of two linear displacements and one torsional displacement. To meet the requirement of aerodynamic modeling, the flutter derivatives of a box girder section are identified, verifying its accuracy and feasibility by comparing with previously reported results. By simulating the nonstationary vibration with time-variant amplitude, the phenomena of frequency multiplication and memory effects are examined. In addition to studying the aerodynamics of a bluff body under large amplitudes and nonstationary vibrations, some potential applications of the proposed FMA are discussed in vehicle-bridge-wind dynamic analysis, pile-soil interaction, and line-tower coupled vibration aerodynamics in structural engineering.

Key words: Forced motion apparatus (FMA); Coupled vibration; Stochastic vibration simulation; Aerodynamic force; Frequency multiplication; Memory effects; Wind engineering; Potential applications
https://doi.org/10.1631/jzus.A1900400 **CLC number:** U441.2

1 Introduction

Wind-induced vibrations of long-span bridges during their life cycles have complex stochastic time-variant responses, which are characterized by large amplitude and coupling with different degrees of freedom (DOFs) (Jain et al., 1996), especially when the increasing span (Chen and Cai, 2003), large attack angles (Ding et al., 2000), and non-synoptic wind field (Miyata et al., 2002) are taken into account. These tendencies challenge the feasibility of traditional equipment in wind tunnel tests, involving free vibration systems (Gao and Zhu, 2015) and forced motion apparatuses (Ukeguchi et al., 1966).

As a solution to this complication, forced motion apparatus (FMA) has been improved to become an effective tool realizing a deeper understanding of the mechanisms of aerodynamics. FMAs have developed from coupling of two DOFs (Cao and Sarkar, 2012) to

‡ Corresponding author
* Project supported by the National Key Research and Development Program of China (Nos. 2018YFC0809600 and 2018YFC0809604), the National Natural Science Foundation of China (No. 51678451), and the Independent Subject of State Key Laboratory of Disaster Reduction in Civil Engineering (No. SLDRCE19-B-11), Tongji University, China
ORCID: Wei CUI, https://orcid.org/0000-0001-7489-923X

three DOFs (Diana et al., 2004) and from small to large amplitudes. In the early stages, FMAs focused on harmonic motion (Chen et al., 2005). When the research was extended to post-flutter (Zhu and Gao, 2015), non-synoptic wind fields (Miyata et al., 2002; Chen et al., 2004), and nonstationary processes (Borri et al., 2002), experimental setups with the capability of driving section models in arbitrary ways were attempted (Siedziako and Øiseth, 2018). These improvements indicate the evolution from stationary to nonstationary driving the investigation of bluff body aerodynamics.

To reproduce complex wind-induced structural vibrations, a novel FMA is proposed and designed. Compared with previous apparatuses, it features more varied motion types based on proportion integration differentiation (PID) technology, so it can re-illustrate even stochastic movements with point to point coincidence between prescribed and simulated data. This paper gives a general introduction to the device's design and its potential applications in wind engineering. First, more attention is paid to available motion types, vibration amplitudes, and a PID closed-loop control method and its validation in terms of accuracy and feasibility. Then, several potential applications in the field of structural wind engineering are discussed, including nonstationary aerodynamics, vehicle-bridge-wind dynamic analysis, pile-soil interaction, and line-tower coupled vibrations.

2 Evolution of FMAs

2.1 Development of FMA performance

The performance of an FMA can be described in terms of the number of DOFs, vibration amplitudes, and motion types. This section discusses the history of FMA development in the field of aerodynamic research.

From the view point of DOFs, early FMAs could drive the model to move at only one single DOF, while later ones had coupled two-DOF functions (Halfman, 1952). Three-DOF modeling of lateral, vertical, and torsional motions was also recently achieved. The coupling of multiple DOFs laid the foundation for the study of multi-modal coupled vibration of bluff and streamlined bodies. Some devices combine the functions of forced vibration and free vibration (Falco et al., 1992).

In terms of vibration amplitude, the maximum amplitude of each DOF gradually increases under the requirements of nonlinear aerodynamic research. The three-DOF large amplitude FMA made by Mitsui Crafts Co. Ltd., Japan (Morishima and Inoue, 1999) has a vertical and lateral amplitude of 500 mm and a torsional amplitude of 55°. The Norwegian University of Science and Technology invented an FMA (Siedziako et al., 2017) which has a lateral and vertical amplitude of 100 mm, and a torsional amplitude that can reach 90°. The novel FMA of Tongji University, China has larger amplitude limits with X=±200 mm, Y=±100 mm, and R_Z=±360° (X is lateral, Y is vertical, and R_Z is torsional amplitude) (Zhan et al., 2017). The higher amplitudes facilitate the study of large amplitude wind-induced vibration and nonlinear aerodynamics for bridge sections under extreme wind conditions.

In terms of motion type, the traditional FMAs can drive only in the form of simple harmonic vibration in a single DOF (Niu and Chen, 2014), and cannot easily reproduce possible stochastic wind-induced vibrations, saying nothing of multi-modal coupling, multi-frequency coupling, and nonstationary vibrations. The realization of different vibration types (Bergmann et al., 2003; Siedziako et al., 2017) based on a series of updated FMAs contributes the simulation and reproduction of complex wind-induced vibrations, especially random vibration, considering coupled DOFs or modes, thereby extending the application range in the wind engineering field. Fig. 1 lists the performance parameters of representative FMA worldwide.

2.2 Development of FMA applications in aerodynamic research

Combining an FMA with wind tunnel tests can be used to study aerodynamic phenomena, such as wind-related effects of flexible structures, which is a complicated aerodynamic process. In addition to simulating and reproducing unsteady structural vibration with large amplitudes, large wind attack angles, and multi-modal coupling, the forced vibration method has several other advantages: (1) it realizes a wider range of reduced wind speeds, (2) it obtains a higher signal-to-noise ratio of test signals, and (3) it directly identifies the self-excited aerodynamic force acting on the model.

FMAs initially appeared in the aviation field and its associated aerodynamic research (Halfman,

Number of DOFs	3
Frequency	0.1–3 Hz
Translational amplitude	0–±20 mm@4 mm
Rotational amplitude	0°–±5°@1°
Motion type	Sinusoidal

(a)

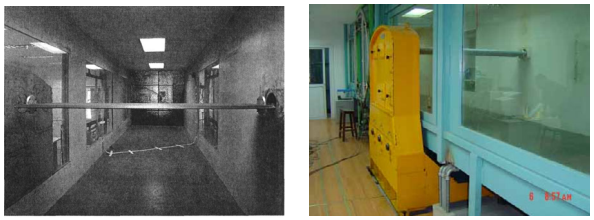

Number of DOFs	3
Frequency	0.1–3 Hz
Translational amplitude	0–±20 mm@4 mm
Rotational amplitude	0°–±5°@1°
Motion type	Sinusoidal

(b)

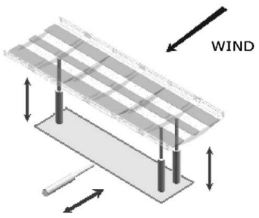

Number of DOFs	2
Frequency	0.025–4 Hz
Motion type	Sinusoidal

(c)

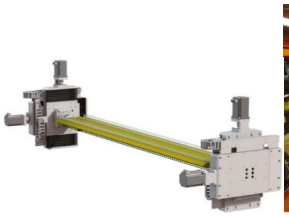

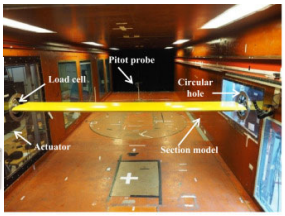

Number of DOFs	3
Lateral and vertical amplitudes	±100 mm
Torsional amplitude	±90°
Amplitude resolution	Continuous
Motion type	Stochastic

(d)

Fig. 1 Schematic of forced motion apparatuses: (a) FMA in Hunan University, China; (b) early FMA in Tongji University, China; (c) FMA in Milan Polytechnic University, Italy; (d) FMA in Norwegian University of Science and Technology, Norway. The symbol @ means the interval step of amplitude increment of FMAs

1952). Early in the 1950s, Halfman (1952) began to use the forced vibration method to test airfoils. The unsteady aerodynamic force of the airfoil was measured for single vertical or torsional vibration and coupled vertical and torsional vibration. Then, Ukeguchi et al. (1966) first applied an FMA to the study of an aerodynamic self-excited force in a bridge section. Since then, a large number of aerodynamic characteristics have been studied. The progress of representative research is shown in Table 1.

3 A novel forced motion apparatus

3.1 Motion types

The framework of our proposed apparatus is shown in Fig. 2. Its essential function is to make models move in designated ways. Three DOFs, namely horizontal (X), vertical (Y), and torsional (R_Z), are driven separately by two linear and one rotational motion actuators. Three DOFs can be arbitrarily coupled through the cooperation of individual linear rails and the rotary axis. The length of the linear rails of the FMA restricts the motion amplitudes. The amplitude limits of X, Y, and R_Z are respectively ±200 mm, ±100 mm, and ±360°. The driving and decoupling mechanical method makes it possible for three DOFs to work independently to realize any complex movements (Fig. 3).

There is no restriction on motion types for any DOF, as long as the required driving forces are within the capacity of the actuators. The motion types stem from single-frequency harmonic vibration and can be summarized as

$$D(t)=\sum_{i=1}^{m}A_i(t)\cdot\sin\left[2\pi\cdot f_i(t)\cdot t+\theta_i(t)\right]+T(t), \quad (1)$$

Table 1 Applications of FMA to research on aerodynamic characteristics

Reference	Section shape	DOF	Aerodynamic force acquired	Study object
Halfman (1952)	Airfoil	Y, R_Z, Y+R_Z	Force	Unsteady aerodynamic force
Ukeguchi et al. (1966)	Bridge		Force	Aerodynamic self-excited force
Otsuki et al. (1974)	Square		Pressure	Aerodynamic nonlinearity
Falco et al. (1992)	Box girder	Y, R_Z, Y+R_Z	Force	Identification of aerodynamic parameters by time domain method
Matsumoto et al. (1993)	1:10 and 1:20 rectangular			Aerodynamic derivatives
Li (1995)	Box girder; twin-side-girder; rectangular	Y, R_Z	Force	Aerodynamic derivatives; comparison of water tunnel and wind tunnel
Cigada et al. (2001)	Box girder		Force	Zasso form of aerodynamic parameters
Chen and Yu (2002)	Flat; side-girder; box girder	Y, R_Z	Force	Nonlinearity of self-excited force
Bergmann et al. (2003)			Force	Aerodynamic derivatives
Diana et al. (2004)	Box girder	Three DOFs	Force	Aerodynamic parameters
Guo (2006)	Thin plate; ribbed plate; box girder	Single DOF +three DOFs	Force	Comparison of time domain and frequency domain method; comparison of single DOF and three DOFs
Niu and Chen (2014)	Thin plate; ribbed plate; box girder	Single DOF +three DOFs	Force	Comparison of time domain and frequency domain method; comparison of single DOF and three DOFs; aerodynamic derivatives; flutter mechanism
Wang (2011)	Bridge girder	Y, R_Z	Force	Nonlinear aerodynamic model
Li et al. (2016)	1:5 rectangular		Pressure	Spanwise correlation of aerodynamic force
Siedziako et al. (2017)	Box girder		Force	Aerodynamic derivatives and characteristics under different motion patterns

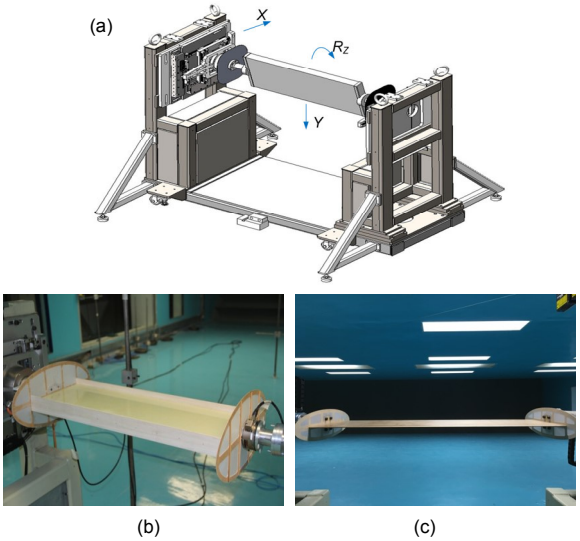

Fig. 2 Images of the novel FMA: (a) schematic of FMA; (b) H-shaped section model; (c) flat section model

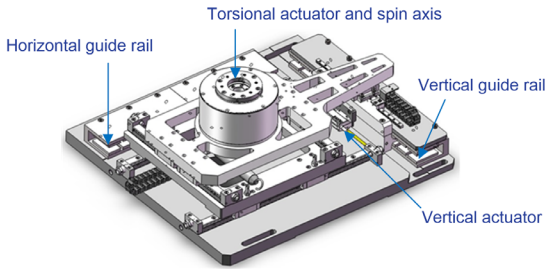

Fig. 3 Driving and decoupling systems of three DOFs

where $D(t)$ is the time history of displacement, $T(t)$ is a global trend term, $A_i(t)$ is the amplitude of the ith component, $f_i(t)$ is the motion frequency of the ith component, $\theta_i(t)$ is the initial phase angle of the ith component, and m is the number of superposed vibration components. $A_i(t)$, $f_i(t)$, $\theta_i(t)$, and $T(t)$ can be expressed as time-variant functions of time to simulate nonstationary or even unsteady vibrations.

Motion types are controlled by pre-generated input data in the form of time series. Typical time series are shown in Fig. 4, including harmonic motion with a single frequency (Fig. 4a) and evolutions

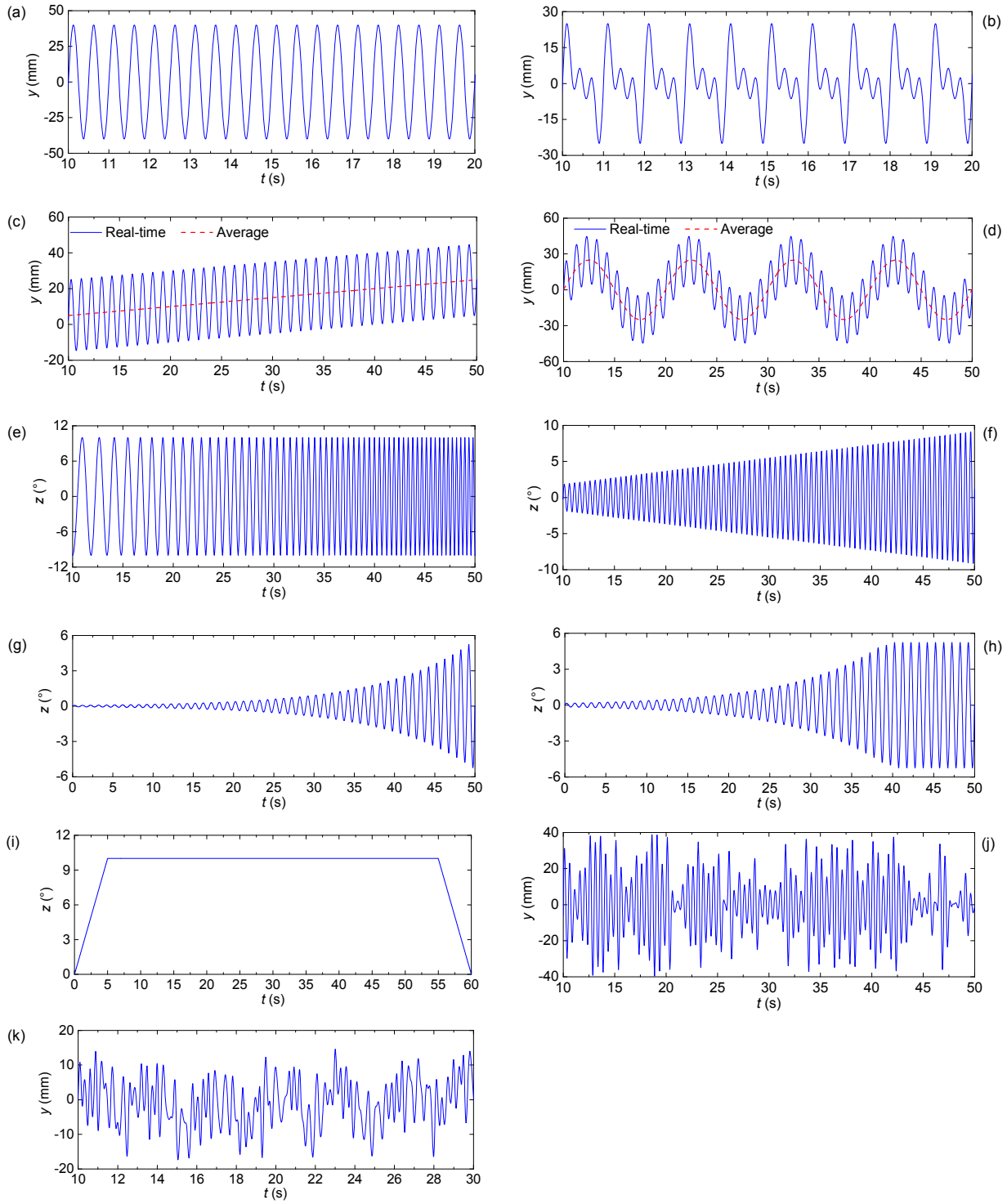

Fig. 4 Typical real-time movements of FMAs: (a) harmonic motion with a single frequency; (b) sinusoid-like motion with multiple frequencies; (c) sinusoid-like motion with a linear time-variant trend; (d) sinusoid-like motion with a harmonic time-variant trend; (e) sinusoid-like motion with time-variant frequency; (f) sinusoid-like motion with a linear time-variant amplitude; (g) sinusoid-like motion with an exponential time-variant amplitude; (h) sinusoid-like motion with a nonlinear time-variant amplitude; (i) motion with an impact and flat stage; (j) sinusoid-like motion with a random amplitude; (k) arbitrary motion

based on it, including multi-frequency (Fig. 4b), time-variant average (Figs. 4c and 4d), time-variant frequency (Fig. 4e), time-variant amplitude (Figs. 4f–4h), flat stage (Fig. 4i), random amplitude (Fig. 4j), and arbitrary motion (Fig. 4k). The various motion types pave the way for the simulation of potential wind-induced vibrations of long-span bridges and high-rise buildings.

3.2 Running accuracy

To perform a comparative study and a parameterization study, it is necessary to accurately reproduce customized motions under different external disturbances. Accuracy is guaranteed by real-time monitoring of running states and adjustments of driving forces (F_D) based on the concept of PID. Laser inspectors are installed inside the apparatus to monitor its current displacements. Driving forces are adjusted automatically according to a comparison of measured displacements (D_m) and expected displacements (D_e). When D_m is smaller than D_e, $F_D(t_{i+1})$ will be reinforced, otherwise, it will be attenuated. The adjustment process is shown in Fig. 5.

To verify the effectiveness of the self-adjustment system illustrated in Fig. 5, section models weighing 1.5 kg and 2.0 kg respectively were forced to move in typical ways under different wind velocities. To be more universal and convincing, the typical motion types shown in Fig. 4 were all tested, combining several amplitudes and frequencies. Variation in model weight, motion amplitude, motion frequency, and incoming wind velocity led to different external disturbances, which required adjustment of driving forces.

Accuracy was quantitatively evaluated by determination of the coefficient R^2 (calculated from Eq. (2)), using the motion without wind as a reference. The distributions of R^2 values are shown in Fig. 6. R^2 values for three DOF values under different verification tests were all very close to 1.0, indicating that the control system works effectively and can resist various obstructions. To be more intuitive, a sinusoid-like motion with random amplitude is presented as an example in Fig. 7.

$$R^2 = 1 - \frac{\sum_{i=1}^{n}\left(y_{u=0,i} - \widehat{y}_{u=U,i}\right)^2}{\sum_{i=1}^{n}\left(y_{u=0,i} - \overline{y}_{u=0}\right)^2}, \tag{2}$$

$$\overline{y}_{u=0} = \frac{1}{n}\sum_{i=1}^{n} y_{u=0,i}, \tag{3}$$

where $y_{u=U,i}$ is the displacement of the ith sampling point under a wind speed of U, $y_{u=0,i}$ is the displacement of the ith sampling point when there is no wind, and n is the total number of sampling points.

4 Identification of flutter derivatives of a typical bluff body section

4.1 Identification method

The Theodorsen self-excitation model is suitable only for thin airfoil or flat sections, not for bluff body sections with significant airflow separation (Wu, 2013). The self-excitation model of a bluff body section is a set of semi-theoretical and semi-empirical formulas. The corresponding aerodynamic parameters must be identified through experimental or numerical analysis. The Scanlan self-excitation model is the most widely used in the wind engineering field.

Scanlan and Tomko (1971) proposed a linear expression of aerodynamic self-excitability expressed by six flutter derivatives H_i^* and A_i^* (i=1–3), the first derivative of the vertical displacement ($\dot{h}$) of the structure, the torsional angle (α), and the first derivative of the torsional angle ($\dot{\alpha}$). Huston (1986) considered the influence of vertical displacement (h) and obtained expressions for aerodynamic lift and moment including eight flutter derivatives. With increasing in bridge spans, the lateral displacement becomes more important in the system of self-excited aerodynamic modelling. Sarkar et al. (1994) extended the self-excited force model to three DOFs (Eq. (4)) by considering the aerodynamic derivatives related to the lateral displacement (p) and the first derivative of the lateral displacement ($\dot{p}$).

$$\begin{aligned} D = \rho U^2 B \cdot \Bigg(& K_p P_1^* \frac{\dot{p}}{U} + K_\alpha P_2^* \frac{B\dot{\alpha}}{U} + K_\alpha^2 P_3^* \alpha \\ & + K_p^2 P_4^* \frac{p}{B} + K_h P_5^* \frac{\dot{h}}{U} + K_h^2 P_6^* \frac{h}{B} \Bigg), \end{aligned} \tag{4a}$$

$$\begin{aligned} L = \rho U^2 B \cdot \Bigg(& K_h H_1^* \frac{\dot{h}}{U} + K_\alpha H_2^* \frac{B\dot{\alpha}}{U} + K_\alpha^2 H_3^* \alpha \\ & + K_h^2 H_4^* \frac{h}{B} + K_p H_5^* \frac{\dot{p}}{U} + K_p^2 H_6^* \frac{p}{B} \Bigg), \end{aligned} \tag{4b}$$

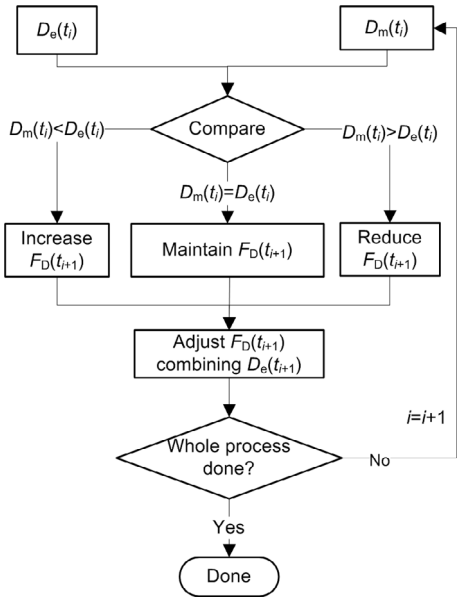

Fig. 5 Closed-loop PID feedback system for running accuracy

$$M=\rho U^2B^2\cdot\left(K_hA_1^*\frac{\dot{h}}{U}+K_\alpha A_2^*\frac{B\dot{\alpha}}{U}+K_\alpha^2A_3^*\alpha+K_h^2A_4^*\frac{h}{B}+K_pA_5^*\frac{\dot{p}}{U}+K_p^2A_6^*\frac{p}{B}\right), \tag{4c}$$

where D, L, and M are the self-excited forces acting on the section model per unit length, which represent drag force, lift force, and moment, respectively. ρ is the air density, B is the width of the bridge section, and U is the wind velocity. K_p, K_h, and K_α are reduced wind velocity in lateral, vertical, and torsional displacements of forced vibration, respectively. P_i^*, H_i^*, and A_i^* (i=1–6) are lateral, vertical, and torsional flutter derivatives, respectively.

The method of the forced vibration time domain (Falco et al., 1992) is used to identify the flutter derivatives, including the single-DOF, two-DOF coupling, and three-DOF coupling. The correspondence between the DOF coupling and the single identifiable flutter derivative is summarized in Table 2. As

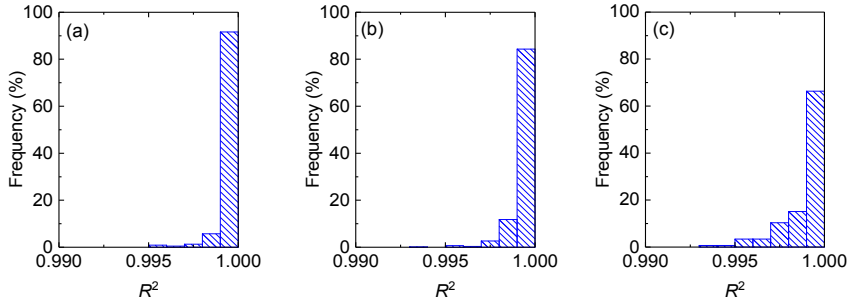

Fig. 6 R^2 value distributions under various types of motion: (a) X; (b) Y; (c) R_Z

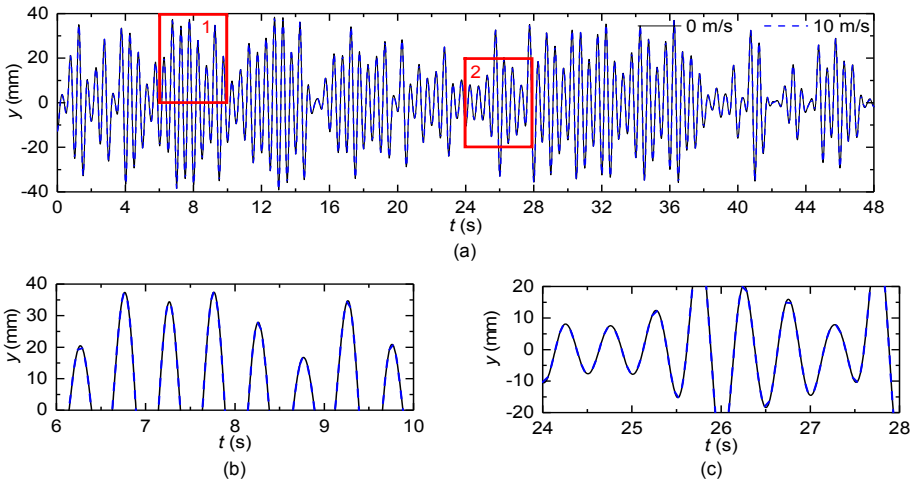

Fig. 7 Running accuracy under different wind velocities: (a) global comparison; (b) local magnification of No. 1; (c) local magnification of No. 2

shown in Table 2, the conditions that can be used for flutter derivative identification are selected from all test conditions.

The identification and calculation formulas of the flutter derivative can be explained by taking the three-DOF coupling condition as an example.

The Scanlan self-excited expression in Eq. (4) is expressed in matrix form as

$$\boldsymbol{F}=\boldsymbol{X}\cdot\boldsymbol{E}, \tag{5}$$

where $\boldsymbol{F}$ is the aerodynamic time history matrix, $\boldsymbol{E}$ is the flutter derivatives matrix, and $\boldsymbol{X}$ is the motion time history matrix.

According to Eq. (4), 18 aerodynamic derivatives can be obtained from the time history of self-excited force on the left and the time history of motion on the right through the least square method at each reduced wind velocity.

$$\boldsymbol{E}=\left(\boldsymbol{X}^{\mathrm{T}}\boldsymbol{X}\right)^{-1}\boldsymbol{X}^{\mathrm{T}}\boldsymbol{F}, \tag{6}$$

Table 2 Relationship between flutter derivatives and DOF coupling

Method	DOF	Related flutter derivatives	Condition
Single DOF	X	$H_5^*, H_6^*, A_5^*, A_6^*, P_1^*, P_4^*$	SHM
	Y	$H_1^*, H_4^*, A_1^*, A_4^*, P_5^*, P_6^*$	SHM
	R_Z	$H_2^*, H_4^*, A_1^*, A_4^*, P_5^*, P_6^*$	SHM
Two DOFs	$X+Y$	$H_1^*, H_4^*, H_5^*, H_6^*, A_1^*, A_4^*, A_5^*, A_6^*, P_1^*, P_4^*, P_5^*, P_6^*$	SHM, $\omega_p\neq\omega_h$
	$X+R_Z$	$H_2^*, H_3^*, H_5^*, H_6^*, A_2^*, A_3^*, A_5^*, A_6^*, P_1^*, P_2^*, P_3^*, P_4^*$	SHM, $\omega_p\neq\omega_\alpha$
	$Y+R_Z$	$H_1^*, H_2^*, H_3^*, H_4^*, A_1^*, A_2^*, A_3^*, A_4^*, P_2^*, P_3^*, P_5^*, P_6^*$	SHM, $\omega_h\neq\omega_\alpha$
Three DOFs	$X+Y+R_Z$	18 flutter derivatives	SHM, $\omega_h\neq\omega_p\neq\omega_\alpha$

Note: SHM it the single-frequency harmonic motion; ω_p, ω_h, and ω_α are lateral, vertical, and torsional circular frequencies of forced vibration, respectively

$$\boldsymbol{F}=\begin{bmatrix}L(t) & D(t) & M(t)\end{bmatrix}=\begin{bmatrix}L(t_1) & D(t_1) & M(t_1)\\ L(t_2) & D(t_2) & M(t_2)\\ \vdots & \vdots & \vdots\\ L(t_n) & D(t_n) & M(t_n)\end{bmatrix}, \tag{7}$$

$$\boldsymbol{E}=\rho U^2 B\cdot\begin{bmatrix}\frac{K_h}{U}H_1^* & \frac{K_\alpha B}{U}H_2^* & K_\alpha^2 H_3^* & \frac{K_h^2}{B}H_4^* & \frac{K_p}{U}H_5^* & \frac{K_p^2}{B}H_6^*\\ \frac{K_p}{U}P_1^* & \frac{K_\alpha B}{U}P_2^* & K_\alpha^2 P_3^* & \frac{K_p^2}{B}P_4^* & \frac{K_h}{U}P_5^* & \frac{K_h^2}{B}P_6^*\\ \frac{K_h B}{U}A_1^* & \frac{K_\alpha B^2}{U}A_2^* & \frac{K_\alpha B^2}{U}A_3^* & K_h^2 A_4^* & \frac{K_p B}{U}A_5^* & K_p^2 A_6^*\end{bmatrix}, \tag{8}$$

4.2 Identification results

Flutter derivative identification is a process of obtaining the dependent relationship between the motion state and the aerodynamic time history in Eq. (9). The aerodynamic time history, Eq. (10), can be derived from the motion state and the flutter derivative. The time history can also be used in this model to evaluate the accuracy of flutter derivative identification. This is done by comparing the aerodynamic time history calculated by the derivation of the flutter derivative with directly measured aerodynamic results. The R^2 value (Eq. (2)) is used as the quantitative evaluation index.

$$\boldsymbol{E}=f\left(\boldsymbol{X},\boldsymbol{F}\right), \tag{9}$$

$$\boldsymbol{F}=g\left(\boldsymbol{X},\boldsymbol{E}\right). \tag{10}$$

The various derivatives identified by different working conditions are rather discrete, and it is necessary to give a fitting curve of multiple recognition results and a confidence interval with a certain guarantee rate.

The geometries of the box section used for the flutter derivative in this section are shown in Table 3.

Table 3 Criteria, confidence interval, and comparison objects of flutter derivatives (unit: mm)

Section type	Lower limit of R^2	Confidence interval	Comparison object	Comparison section
Box girder	0.90	95%	Wind tunnel tests (Chen et al., 2005) Wind tunnel tests (Niu, 2008) Computational fluid dynamics (Ying, 2017)	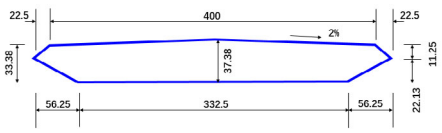

A box girder section was selected, and its cubic polynomial fitting curve and confidence interval with 95% guarantee rate are shown in Fig. 8. The horizontal coordinate is the reduced wind speed $U/(fB)$, where f is the frequency, and the vertical coordinate is flutter derivative. The fitting curve and its confidence interval are compared with other published results, and the data sources for comparison are shown in Table 3.

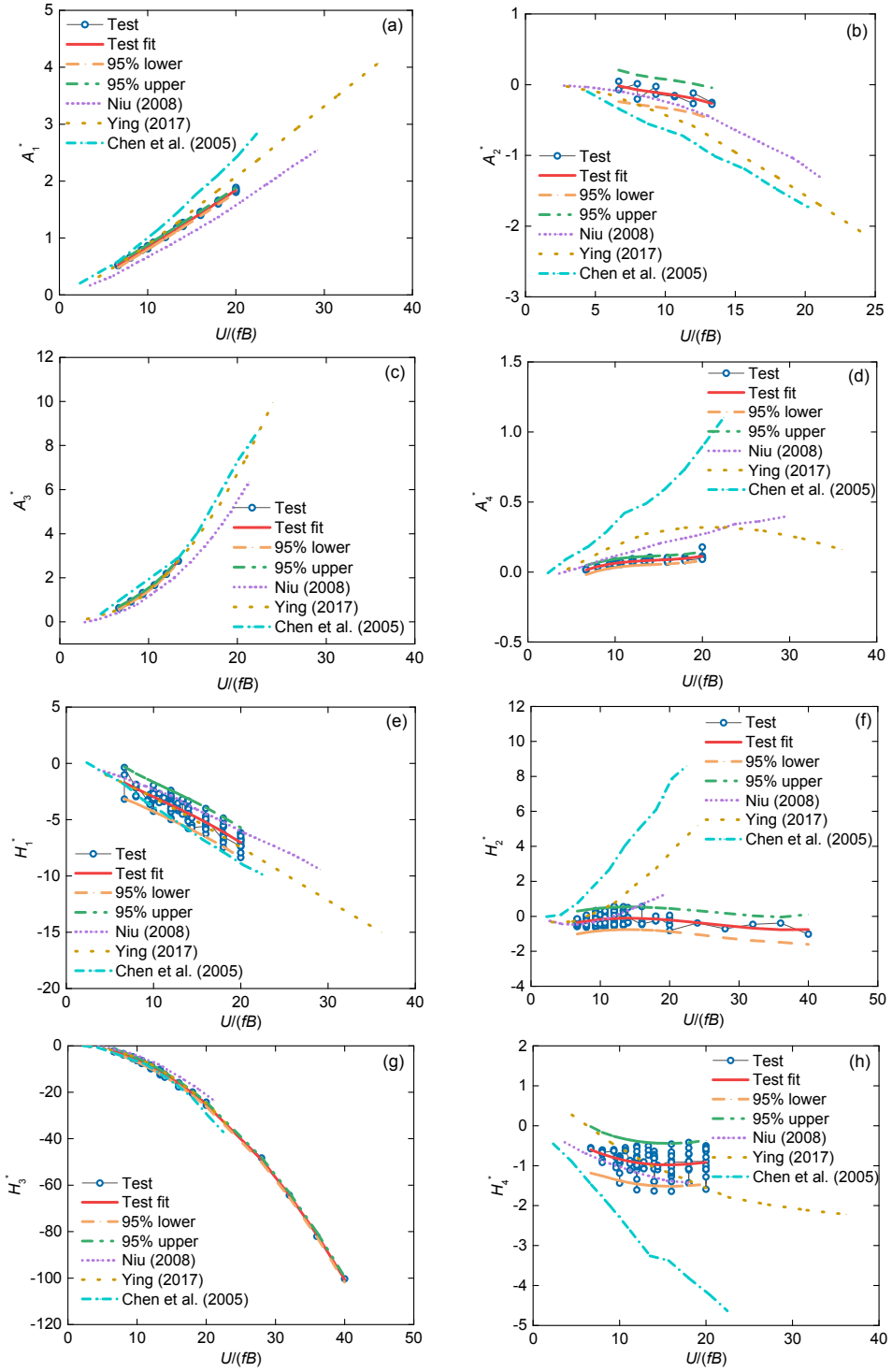

Fig. 8 Identification results of flutter derivatives of a typical box girder section: (a) A_1^*; (b) A_2^*; (c) A_3^*; (d) A_4^*; (e) H_1^*; (f) H_2^*; (g) H_3^*; (h) H_4^*

5 Extended application in structural engineering

5.1 Nonlinear and nonstationary aerodynamic forces and aerodynamic characteristics

Structural vibration and wind fluctuation collectively contribute to aerodynamic force. One aim of bridge wind resistance research is to establish a relationship among the three (Davenport, 1962; Scanlan and Gade, 1977; Scanlan, 1993). Traditionally, structural vibrations are mostly within the scope of single-frequency and small-amplitude harmonic motion; the wind field is usually produced by passively-controlled wind tunnels. However, for ultra-long-span bridges across the sea (Miyata et al., 2002; Ge et al., 2018b), it is not enough to consider merely small-amplitude vibration and the synoptic wind field. More complex coupled structural movements and non-synoptic wind environments such as typhoons and tornados should be paid more attention (Fig. 9). Aerodynamic forces under these conditions can be studied by combining FMAs with actively-controlled wind tunnels (Cao et al., 2001; Ma et al., 2013). FMAs can simulate the contribution of large-amplitude, multi-mode, multi-frequency, and nonstationary vibrations. Actively-controlled wind tunnels can be used to model nonstationary and extreme wind environments.

An application of the device to aerodynamic force research is illustrated in Fig. 10, where the section model is given prescribed vibrations and various wind fields can be simulated through wind tunnels. The relationship and interaction mechanisms among wind, structure vibration, and aerodynamic forces can be revealed by proper mathematical tools. The effects of a large attack of angles, large vibration amplitudes, complex vibration forms, and special wind fields can be clearly understood for proper wind resistance design.

In addition to long-span bridges, the FMA can be applied to the aerodynamics of rotating flying objects. Taking full advantage of 360° continuous rotation, large angle flips of flying aircraft (Nielsen, 2015) can be simulated and corresponding aerodynamic forces measured (Fig. 11).

The FMA can also be applied to a nonlinear or nonstationary aerodynamic force like the identification of admittance. Earlier models based on wind tunnel tests or theory can identify the admittance under the incoming turbulence (Zhao and Ge, 2015). By using the FMA, the extreme wind environment can be realized to identify the admittance and possibly build a reasonable framework.

In this paper, we take harmonic vibration with time-variant amplitude as an example, briefly introducing the aerodynamic nonstationary characteristics of a typical bluff body section. According to preliminary experimental data analysis, the torsional

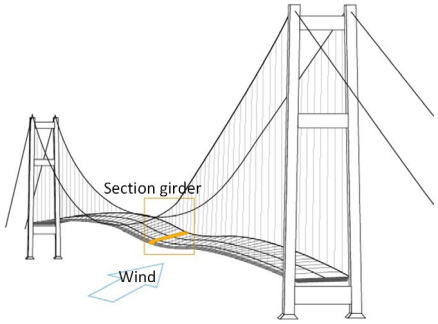

Fig. 9 Amplitude-dependent aerodynamics of a long-span bridge under a stochastic wind field

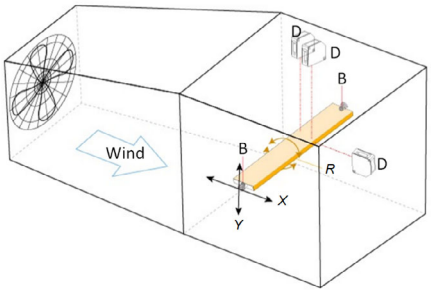

Fig. 10 Application to the study of aerodynamic forces on a bluff body (B stands for force-measurement balance and D for displacement-measurement sensor)

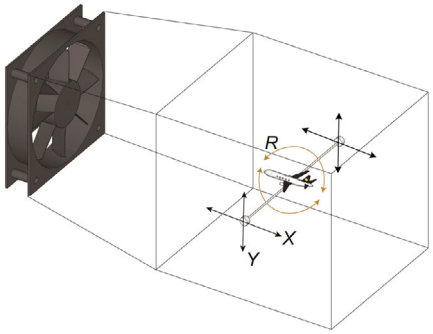

Fig. 11 Application to the study of the aerodynamics of flying aircraft

nonstationary vibration is more likely to cause a nonstationary aerodynamic force than vertical vibration. Therefore, the torsional force is used for data analysis and explanation. In time-variant amplitude vibration, the motion frequency does not change with time, but the motion amplitude increases or decreases regularly with time.

For the nonstationary process in Fig. 12, three time history curves represent torsional displacement, aerodynamic force, and aerodynamic work under the case of 10 m/s. The aerodynamics show a synchronous developing tendency with vibration input, and when the amplitude increases to a certain value, the aerodynamic force shows apparent frequency multiplication, with a threshold at a specific moving amplitude. This phenomenon reflects the amplitude dependence of aerodynamic force.

To evaluate memory effects, two reverse vibrations are compared under different wind velocities from 5 m/s to 10 m/s (Fig. 13). The motion frequency and the maximum displacement amplitude are the same, but the displacement amplitude (Fig. 13a) increases linearly with time from 24 s to 48 s, while the displacement amplitude (Fig. 13b) decreases linearly in the same time interval. It can be seen from the graph that the symbols and absolute values of aerodynamic torque work (W') are similar in the two reverse processes, but the shapes of the aerodynamic work time history curves are different. In conclusion, the dimensionless work curves show obvious asymmetric development, meaning that reverse vibration did not induce reverse aerodynamic force and the conversion from vibration to aerodynamic was irreversible, which is a typical evidence about aerodynamic memory effects depending on the former aerodynamic evolution process.

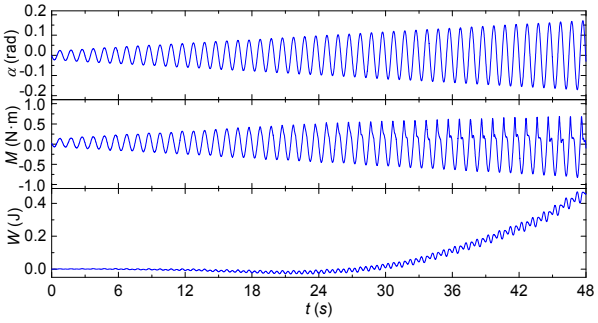

Fig. 12 Time history of torsional displacement, aerodynamic force, and aerodynamic work (W)

In conclusion, the FMA can be used to model nonstationary aerodynamic phenomena, including extreme time-variant wind speed, frequency multiplication, the identification of admittance, amplitude-dependent, and even track-dependent effects of aerodynamic work, but further research is needed.

5.2 Vehicle-bridge-wind dynamic analysis

According to present practice, long-span bridges are closed to limit traffic only when wind velocities are above a prescribed wind speed threshold. Consequently, it is normal for the wind, bridge, and vehicles to interact with each other under normal running states (Fig. 14). The existence of moving vehicles changes the aerodynamic shapes of structures and consequently influences their wind-induced responses. Furthermore, the dynamic responses of the bridge are transferred to passing vehicles (Xu and Guo, 2003), leading to the problem of driving comfort (Guo and Xu, 2006) and operational difficulties. The study of vehicle-bridge-wind coupling effects is instructive in the evaluation of structural aerodynamic stability, driving comfort and determination of driving speed limits to avoid conservative traffic limitation.

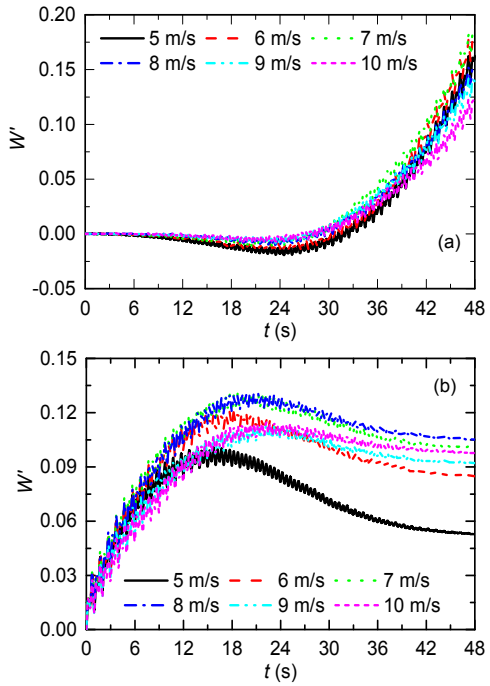

Fig. 13 Time history curve of aerodynamic torque work (W') of a box girder section: (a) α_{max}=0°–11°, f=1 Hz; (b) α_{max}=11°–0°, f=1 Hz (dimensionless results)

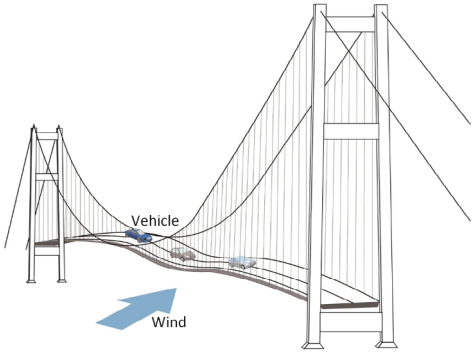

Fig. 14 Vehicle-bridge-wind coupling problem

At present, vehicle-bridge-wind coupling problems are generally analyzed through numerical simulation (Xu and Guo, 2003; Cai and Chen, 2004; Calçada et al., 2005) while wind tunnel tests are relatively rare (Calçada et al., 2005). The lack of wind tunnel tests is partly due to the complexity of experimental systems involving moving vehicles, vibrating girders, and various cross-bridge winds. System performance is evaluated from different perspectives, including bridge safety and driver comfort (Cai and Chen, 2004).

The experimental setup related to this application is illustrated in Fig. 15. The wind field can be re-produced by passively or actively controlled turbulence-generating wind tunnels. Wind-induced vibrations of a bridge deck are simulated by an FMA. A vehicle is driven by bridge girder models through elastic connections. Driving speed and wind velocity can be simply simulated by adjusting the angle between the section model axis and incoming flow. Effects of moving vehicle groups can be studied through different combinations of the number, type, and position of vehicle models. To study driver comfort and operational difficulty, it is necessary to simulate not only the aerodynamic shapes of vehicles, but also their mass, damping, and stiffness systems (Cai and Chen, 2004). With the help of the proposed FMA, more attention can be paid to the simulation of the vehicle system compared with a 3D bridge model of wind-induced vibration. From the perspective of vehicles, section models of bridge girders play a role as a shaker, which can easily simulate more complex stationary or nonstationary movements.

5.3 Pile-soil interaction under wind-induced vibration

Wind directly affects the superstructures of high-rise buildings, transmission towers, and tall bridge towers, and their dynamic responses are transferred to group-pile foundations (Fig. 16), leading to pile-soil interaction (Damgaard et al., 2014). However, present wind engineering focuses mainly on superstructures and ignores substructures.

FMAs are applied to simulate equivalent vibrations at the junctions of superstructures and substructures, and can be adopted to study dynamic pile-soil interaction.

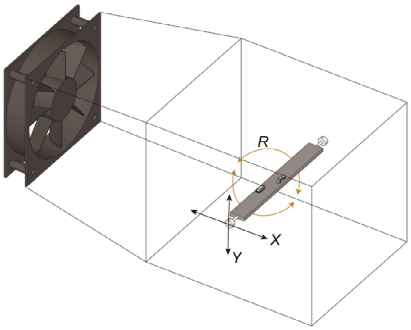

Fig. 15 Application to vehicle-bridge-wind coupling analysis

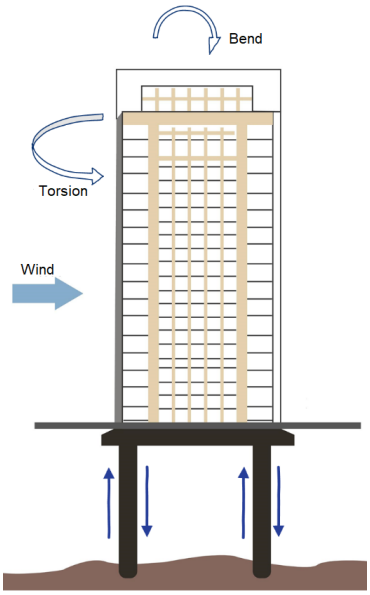

Fig. 16 Pile-soil interaction considering wind effect simulation excitation

An experimental setup of this application is illustrated in Fig. 17. The apparatus is used to simulate equivalent dynamic responses of superstructures, which can be determined from field measurements, wind tunnel tests, and FEM analysis. The vibrations are filtered and transferred to substructures through elastic connections, whose stiffness depends on specific situations. In addition to wind engineering, it is applicable to other dynamic effects, such as earthquake effects (Gazetas and Makris, 1991; Makris and Gazetas,1992) and bursting loads.

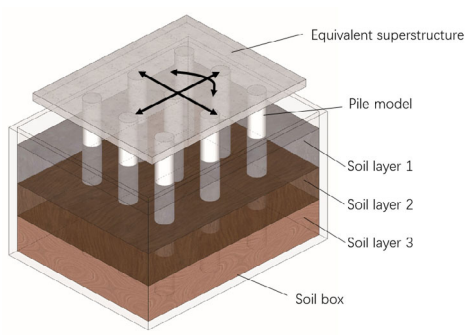

Fig. 17 Application to the study of pile-soil interaction under simulation excitation

5.4 Line-tower coupled vibration of transmission tower

Transmission towers are more flexible than general high-rise buildings. Additionally, spans between adjacent towers are generally large. Consequently, towers and lines are coupled under distinctive dynamic characteristics, which makes it improper to treat them separately. It is necessary to consider the interaction between towers and lines (Li and Bai, 2006). Line-tower interaction problems are illustrated in Fig. 18.

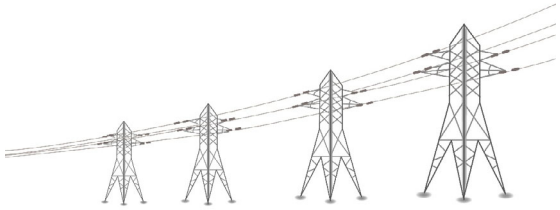

Fig. 18 Interaction between transmission towers and lines

In terms of tower-line coupled vibration, present research methods are mainly aeroelastic-model wind tunnel tests (Loredo-Souza and Davenport, 2001; Huang et al., 2012; Liang et al., 2015) and numerical simulations (Ghobarah et al., 1996; Battista et al., 2003; Zhang et al., 2013). Adjacent transmission towers are generally far apart and lines are rather thin. However, the dimensions of wind tunnels are limited, which makes simulation in a wind tunnel test difficult. Numerical simulations require validation of physical wind tunnel tests. Forced motion devices provide an effective alternative as a movable boundary restriction.

Taking lines as research targets, the application is shown in Fig. 19. The device is used to simulate the vibration at the junction of towers and a line, including vibrations in along-line and cross-line directions. The line system is simulated through an approximate model that satisfies similar criteria. Dynamic responses of the line-tower system are closely related to boundary conditions (Ghobarah et al., 1996), and vibrations of side transmission towers may not be exactly the same due to differences among engineering sites. Under this condition, the vibrations in the two directions need to be controlled separately.

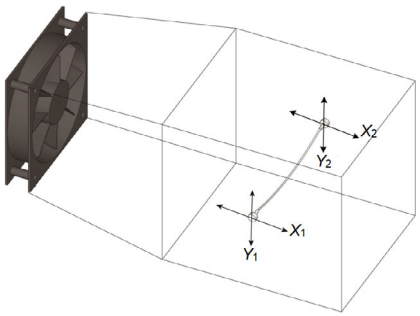

Fig. 19 Application to line-tower coupled vibration considering boundary simulation movement

In addition to wind-induced vibration, the setup shown in Fig. 16 can be used in combination with other factors. Many transmission towers under construction or design in China are faced with coupled phenomena, such as wind-sand (Kikuchi et al., 2003), wind-rain (Kikuchi et al., 2003; Ge et al., 2018a), wind-snow (Zhou et al., 2016), and wind-ice (Pospíšil et al., 2016). The effects of coupled factors can be simulated by the combination of the apparatus, wind tunnels, and other devices.

6 Conclusions

An FMA has been developed based on the PID control algorithm to simulate different forms of wind-induced vibrations. Various motion types are realized in individual DOFs and coupling two even three DOFs, including stationary and nonstationary DOFs. Running accuracy is verified under different external obstructions by tests for a variety of wind loads and different driven weights. The rationality of the application of the FMA in the wind engineering field has been verified by identifying and comparing the flutter derivatives of a box girder section. Simulation of various motion types paves the way for its application in structural wind engineering, including nonstationary aerodynamic forces, vehicle-bridge-wind coupling vibration, pile-soil interaction, and line-tower coupled vibrations.

Contributors

Lin ZHAO wrote the manuscript. Xi XIE did the wind tunnel tests and calculated the data about flutter derivatives. Yan-yan ZHAN provided the data of various vibrations and their accuracy based on the FMA. Wei CUI and Yao-jun GE provided the suggestions on the framework of this paper. Zheng-chun XIA, Sheng-qiao XU, and Min ZENG gave some important advice about the feasibility of the extended applications of the FMA.

Conflict of interest

Lin ZHAO, Xi XIE, Yan-yan ZHAN, Wei CUI, Yao-jun GE, Zheng-chun XIA, Sheng-qiao XU, and Min ZENG declare that they have no conflict of interest.

References

Battista RC, Rodrigues RS, Pfeil MS, 2003. Dynamic behavior and stability of transmission line towers under wind forces. *Journal of Wind Engineering and Industrial Aerodynamics*, 91(8):1051-1067. https://doi.org/10.1016/S0167-6105(03)00052-7

Bergmann D, Kaiser U, Wagner S, 2003. Determination of flutter derivatives using the forced oscillation method with a stochastical white noise excitation. Proceedings of the 11th International Conference on Wind Engineering.

Borri C, Costa C, Zahlten W, 2002. Non-stationary flow forces for the numerical simulation of aeroelastic instability of bridge decks. *Computers & Structures*, 80(12):1071-1079. https://doi.org/10.1016/S0045-7949(02)00066-4

Cai CS, Chen SR, 2004. Framework of vehicle–bridge–wind dynamic analysis. *Journal of Wind Engineering and Industrial Aerodynamics*, 92(7-8):579-607. https://doi.org/10.1016/j.jweia.2004.03.007

Calçada R, Cunha A, Delgado R, 2005. Analysis of traffic-induced vibrations in a cable-stayed bridge. Part II: numerical modeling and stochastic simulation. *Journal of Bridge Engineering*, 10(4):386-397.

Cao BC, Sarkar PP, 2012. Identification of rational functions using two-degree-of-freedom model by forced vibration method. *Engineering Structures*, 43:21-30. https://doi.org/10.1016/j.engstruct.2012.05.003

Cao SY, Nishi A, Hirano K, et al., 2001. An actively controlled wind tunnel and its application to the reproduction of the atmospheric boundary layer. *Boundary-Layer Meteorology*, 101(1):61-76. https://doi.org/10.1023/A:1019288828837

Chen J, Xu YL, Zhang RC, 2004. Modal parameter identification of Tsing Ma suspension bridge under Typhoon Victor: EMD-HT method. *Journal of Wind Engineering and Industrial Aerodynamics*, 92(10):805-827. https://doi.org/10.1016/j.jweia.2004.04.003

Chen SR, Cai CS, 2003. Evolution of long-span bridge response to wind-numerical simulation and discussion. *Computers & Structures*, 81(21):2055-2066. https://doi.org/10.1016/S0045-7949(03)00261-X

Chen ZQ, Yu XD, 2002. A new method for measuring flutter self-excited forces of long-span bridges. *China Civil Engineering Journal*, 35(5):34-41 (in Chinese). https://doi.org/10.3321/j.issn:1000-131X.2002.05.008

Chen ZQ, Yu XD, Yang G, et al., 2005. Wind-induced self-excited loads on bridges. *Journal of Structural Engineering*, 131(12):1783-1793. https://doi.org/10.1061/(asce)0733-9445(2005)131:12(1783)

Cigada A, Falco M, Zasso A, 2001. Development of new systems to measure the aerodynamic forces on section models in wind tunnel testing. *Journal of Wind Engineering and Industrial Aerodynamics*, 89(7-8):725-746. https://doi.org/10.1016/S0167-6105(01)00075-7

Damgaard M, Zania V, Andersen LV, et al., 2014. Effects of soil–structure interaction on real time dynamic response of offshore wind turbines on monopiles. *Engineering Structures*, 75:388-401. https://doi.org/10.1016/j.engstruct.2014.06.006

Davenport AG, 1962. Buffeting of a suspension bridge by storm winds. *Journal of the Structural Division*, 88(3):233-270.

Diana G, Resta F, Zasso A, et al., 2004. Forced motion and free motion aeroelastic tests on a new concept dynamometric section model of the Messina suspension bridge. *Journal of Wind Engineering and Industrial Aerodynamics*, 92(6):441-462. https://doi.org/10.1016/j.jweia.2004.01.005

Ding Q, Lee PKK, Lo SH, 2000. Time domain buffeting analysis of suspension bridges subjected to turbulent wind with effective attack angle. *Journal of Sound and Vibration*, 233(2):311-327. https://doi.org/10.1006/jsvi.1999.2801

Falco M, Curami A, Zasso A, 1992. Nonlinear effects in sectional model aeroelastic parameters identification.

Journal of Wind Engineering and Industrial Aerodynamics, 42(1-3):1321-1332. https://doi.org/10.1016/0167-6105(92)90140-6

Gao GZ, Zhu LD, 2015. Nonlinearity of mechanical damping and stiffness of a spring-suspended sectional model system for wind tunnel tests. *Journal of Sound and Vibration*, 355:369-391. https://doi.org/10.1016/j.jsv.2015.05.033

Gazetas G, Makris N, 1991. Dynamic pile-soil-pile interaction. Part I: analysis of axial vibration. *Earthquake Engineering & Structural Dynamics*, 20(2):115-132. https://doi.org/10.1002/eqe.4290200203

Ge YJ, Chang Y, Xu LS, et al., 2018a. Experimental investigation on spatial attitudes, dynamic characteristics and environmental conditions of rain–wind-induced vibration of stay cables with high-precision raining simulator. *Journal of Fluids and Structures*, 76:60-83. https://doi.org/10.1016/j.jfluidstructs.2017.09.006

Ge YJ, Xia JL, Zhao L, et al., 2018b. Full aeroelastic model testing for examining wind-induced vibration of a 5,000 m spanned suspension bridge. *Frontiers in Built Environment*, 4:20. https://doi.org/10.3389/fbuil.2018.00020

Ghobarah A, Aziz TS, El-Attar M, 1996. Response of transmission lines to multiple support excitation. *Engineering Structures*, 18(12):936-946. https://doi.org/10.1016/S0141-0296(96)00020-X

Guo WH, Xu YL, 2006. Safety analysis of moving road vehicles on a long bridge under crosswind. *Journal of Engineering Mechanics*, 132(4):438-446. https://doi.org/10.1061/(asce)0733-9399(2006)132:4(438)

Guo ZS, 2006. Three Degree-of-freedom Forced Vibration Method for Identification of Aerodynamic Derivatives of Bridge Decks. PhD Thesis, Tongji University, Shanghai, China (in Chinese).

Halfman RL, 1952. Experimental Aerodynamic Derivatives of a Sinusoidally Oscillating Airfoil in Two-dimensional Flow. Technical Report Archive & Image Library.

Huang MF, Lou WJ, Yang L, et al., 2012. Experimental and computational simulation for wind effects on the Zhoushan transmission towers. *Structure and Infrastructure Engineering*, 8(8):781-799. https://doi.org/10.1080/15732479.2010.497540

Huston DR, 1986. The Effects of Upstream Gusting on the Aeroelastic Behavior of Long Suspended-span Bridges. PhD Thesis, Princeton University, Princeton, USA.

Jain A, Jones NP, Scanlan RH, 1996. Coupled aeroelastic and aerodynamic response analysis of long-span bridges. *Journal of Wind Engineering and Industrial Aerodynamics*, 60:69-80. https://doi.org/10.1016/0167-6105(96)00024-4

Kikuchi N, Matsuzaki Y, Yukino T, et al., 2003. Aerodynamic drag of new-design electric power wire in a heavy rainfall and wind. *Journal of Wind Engineering and Industrial Aerodynamics*, 91(1-2):41-51. https://doi.org/10.1016/S0167-6105(02)00334-3

Li HN, Bai HF, 2006. High-voltage transmission tower-line system subjected to disaster loads. *Progress in Natural Science*, 16(9):899-911. https://doi.org/10.1080/10020070612330087

Li MS, Li SP, Liao HL, et al., 2016. Spanwise correlation of aerodynamic forces on oscillating rectangular cylinder. *Journal of Wind Engineering and Industrial Aerodynamics*, 154:47-57. https://doi.org/10.1016/j.jweia.2016.04.003

Li QC, 1995. Measuring flutter derivatives for bridge sectional models in water channel. *Journal of Engineering Mechanics*, 121(1):90-101. https://doi.org/10.1061/(asce)0733-9399(1995)121:1(90)

Liang SG, Zou LH, Wang DH, et al., 2015. Investigation on wind tunnel tests of a full aeroelastic model of electrical transmission tower-line system. *Engineering Structures*, 85:63-72. https://doi.org/10.1016/j.engstruct.2014.11.042

Loredo-Souza AM, Davenport AG, 2001. A novel approach for wind tunnel modelling of transmission lines. *Journal of Wind Engineering and Industrial Aerodynamics*, 89(11-12):1017-1029. https://doi.org/10.1016/S0167-6105(01)00096-4

Ma TT, Zhao L, Cao SY, et al., 2013. Investigations of aerodynamic effects on streamlined box girder using two-dimensional actively-controlled oncoming flow. *Journal of Wind Engineering and Industrial Aerodynamics*, 122:118-129. https://doi.org/10.1016/j.jweia.2013.07.011

Makris N, Gazetas G, 1992. Dynamic pile-soil-pile interaction. Part II: lateral and seismic response. *Earthquake Engineering & Structural Dynamics*, 21(2):145-162. https://doi.org/10.1002/eqe.4290210204

Matsumoto M, Shiraishi N, Shirato H, et al., 1993. Aerodynamic derivatives of coupled/hybrid flutter of fundamental structural sections. *Journal of Wind Engineering and Industrial Aerodynamics*, 49(1-3):575-584. https://doi.org/10.1016/0167-6105(93)90051-O

Miyata T, Yamada H, Katsuchi H, et al., 2002. Full-scale measurement of Akashi–Kaikyo Bridge during typhoon. *Journal of Wind Engineering and Industrial Aerodynamics*, 90(12-15):1517-1527. https://doi.org/10.1016/S0167-6105(02)00267-2

Morishima H, Inoue H, 1999. The unsteady aerodynamic force measurement system with forced oscillation of large amplitude. *Wind Engineers, JAWE*, (78):95-97 (in Japanese). https://doi.org/10.5359/jawe.1999.95

Nielsen JN, 2015. Missile aerodynamics–past, present, future. *Journal of Spacecraft and Rockets*, 17(3):165-176. https://doi.org/10.2514/3.57725

Niu HW, 2008. The Research on Three Degree-of-freedom Forced Vibration Method for Identification of Aerodynamic Derivatives and Flutter Mechanism. PhD Thesis, Hunan University, Changsha, China (in Chinese).

Niu HW, Chen ZQ, 2014. Three degrees-of-freedom forced vibration method for identifying eighteen flutter derivatives of bridge decks. *China Civil Engineering Journal*, 47(4):75-83 (in Chinese).

https://doi.org/10.15951/j.tmgcxb.2014.04.003
Otsuki Y, Washizu K, Tomizawa H, et al., 1974. A note on the aeroelastic instability of a prismatic bar with square section. *Journal of Sound and Vibration*, 34(2):233-248. https://doi.org/10.1016/S0022-460X(74)80307-X
Pospíšil S, Trush A, Kuznetsov S, et al., 2016. Influence of wind angle of attack and isotropic turbulence on wind-induced vibrations of ice-accreted bridge cables. Proceedings of the 8th International Colloquium on Bluff Body Aerodynamics and Applications.
Sarkar PP, Jones NP, Scanlan RH, 1994. Identification of aeroelastic parameters of flexible bridges. *Journal of Engineering Mechanics*, 120(8):1718-1742. https://doi.org/10.1061/(asce)0733-9399(1994)120:8(1718)
Scanlan RH, 1993. Problematics in formulation of wind-force models for bridge decks. *Journal of Engineering Mechanics*, 119(7):1353-1375. https://doi.org/10.1061/(asce)0733-9399(1993)119:7(1353)
Scanlan RH, Tomko JJ, 1971. Airfoil and bridge deck flutter derivatives. *Journal of the Engineering Mechanics Division*, 97(6):1717-1737.
Scanlan RH, Gade RH, 1977. Motion of suspended bridge spans under gusty wind. *Journal of the Structural Division*, 103(ST9):1867-1883.
Siedziako B, Øiseth O, 2018. An enhanced identification procedure to determine the rational functions and aerodynamic derivatives of bridge decks. *Journal of Wind Engineering and Industrial Aerodynamics*, 176:131-142. https://doi.org/10.1016/j.jweia.2018.03.025
Siedziako B, Øiseth O, Rønnquist A, 2017. An enhanced forced vibration rig for wind tunnel testing of bridge deck section models in arbitrary motion. *Journal of Wind Engineering and Industrial Aerodynamics*, 164:152-163. https://doi.org/10.1016/j.jweia.2017.02.011
Ukeguchi N, Sakata H, Nishitani H, 1966. An investigation of aeroelastic instability of suspension bridges. Proceedings of Suspension Bridges Symposium.
Wang Q, 2011. The Study on Nonlinear Motion-induced Aerodynamic Force and Nonlinear Aerodynamic Stability of Long-span Bridge Girder. PhD Thesis, Southwest Jiaotong University, Chengdu, China (in Chinese).
Wu T, 2013. Nonlinear Bluff-body Aerodynamics. PhD Thesis, University of Notre Dame, Notre Dame, USA.
Xu YL, Guo WH, 2003. Dynamic analysis of coupled road vehicle and cable-stayed bridge systems under turbulent wind. *Engineering Structures*, 25(4):473-486. https://doi.org/10.1016/S0141-0296(02)00188-8
Ying XY, 2017. Numerical Simulation of Flutter Performance of Long-span Bridges. PhD Thesis, Dalian University of Technology, Dalian, China (in Chinese).
Zhan Y, Zhao S, Zhao L, et al., 2017. Aerodynamic effect of non-stationary motion conditions of typical box girder sections. Proceedings of the 4th National Forum on Wind Engineering for Graduate Students (in Chinese).
Zhang T, Lin YY, Bai HF, 2013. Numerical analysis of transmission towers-lines construction on wind forces. *Journal of Applied Sciences*, 13(9):1587-1591. https://doi.org/10.3923/jas.2013.1587.1591
Zhao L, Ge YJ, 2015. Cross-spectral recognition method of bridge deck aerodynamic admittance function. *Earthquake Engineering and Engineering Vibration*, 14(4):595-609. https://doi.org/10.1007/s11803-015-0048-8
Zhou XY, Qiang SG, Peng YS, et al., 2016. Wind tunnel test on responses of a lightweight roof structure under joint action of wind and snow loads. *Cold Regions Science and Technology*, 132:19-32. https://doi.org/10.1016/j.coldregions.2016.09.011
Zhu LD, Gao GZ, 2015. Influential factors of soft flutter phenomenon for typical bridge deck sections. *Journal of Tongji University (Natural Science)*, 43(9):1289-1294 (in Chinese). https://doi.org/10.11908/j.issn.0253-374x.2015.09.001

中文概要

题　目： 一种在结构工程中具有潜在应用前景的新型强迫运动装置

目　的： 探究新型强迫振动装置在风工程领域的发展与应用。

创新点： 1. 提出一种强迫振动装置，以实现多自由度耦合效应的非线性非平稳气运动，并探讨该装置的应用前景。2. 该装置对运动形式无限制，且振幅及频率均可连续变化，因此所需最大驱动力不超过电机限值即可；不同运动形式在每个自由度上均可实现；对三个自由度之间的组合没有限制，单自由度、任意两自由度耦合和三自由度耦合均可。

方　法： 1. 为模拟不同形式的风振，基于比例-积分-微分（PID）控制算法开发一种强迫振动装置（FMA），并采用自主研发的强迫振动装置实现多自由度耦合的多种强迫振动运动方式。2. 为满足气动建模的要求，采用强迫振动时域法对箱梁截面的颤振导数进行识别，包括单自由度、二自由度和三自由度等多种耦合形式，并与已有的研究结果进行比较，验证该强迫振动装置的准确性和可行性。3. 根据强迫振动装置的特点分析其在风工程领域的应用以及未来的发展应用前景。

结　论： 1. 该强迫运动装置实现了各种运动类型，并通过试验验证了其运行精度；通过对箱梁截面颤振导数的识别和比较，验证了其在风工程领域应用的合理性。2. 该装置还可用于处理其他结构工程领域的问题，如大跨桥梁的风-车-桥耦合问题、输电线塔的塔-线耦合振动问题、飞行物在特定旋转轨迹下的气动力问题和结构风致振动引起的桩-土共同作用等。

关键词： 强迫运动装置；耦合振动；随机振动模拟；气动力；倍频效应；记忆效应；风工程；潜在应用